THE JOURNAL OF BIOLOGICAL CHEMISTRY VOL. 288, NO. 37, pp. 26955–26966, September 13, 2013

Ca^{2+} Influx through Store-operated Ca^{2+} Channels Reduces Alzheimer Disease β-Amyloid Peptide Secretion*[S]

Received for publication, April 15, 2013, and in revised form, July 30, 2013 Published, JBC Papers in Press, July 31, 2013, DOI 10.1074/jbc.M113.473355

William Zeiger[‡], Kulandaivelu S. Vetrivel[‡], Virginie Buggia-Prévot[‡], Phuong D. Nguyen[§], Steven L. Wagner[§], Mitchel L. Villereal[¶1], and Gopal Thinakaran[‡2]

From the [‡]Departments of Neurobiology, Neurology, and Pathology and [¶]Department of Pharmacological and Physiological Sciences, The University of Chicago, Chicago, Illinois 60637 and [§]Department of Neurosciences, University of California, San Diego, La Jolla, California 92037

Background: Dysregulation of Ca^{2+} homeostasis has been implicated in Alzheimer disease pathogenesis, but the effects of Ca^{2+} on amyloid precursor protein processing are not well understood.
Results: Constitutive activation of the store-operated calcium entry pathway reduces β-amyloid generation.
Conclusion: Elevation of Ca^{2+} influx affects amyloid precursor protein processing.
Significance: Alteration of Ca^{2+} homeostasis in Alzheimer disease may influence pathogenesis directly through modulation of β-amyloid production.

Alzheimer disease (AD), the leading cause of dementia, is characterized by the accumulation of β-amyloid peptides (Aβ) in senile plaques in the brains of affected patients. Many cellular mechanisms are thought to play important roles in the development and progression of AD. Several lines of evidence point to the dysregulation of Ca^{2+} homeostasis as underlying aspects of AD pathogenesis. Moreover, direct roles in the regulation of Ca^{2+} homeostasis have been demonstrated for proteins encoded by familial AD-linked genes such as *PSEN1*, *PSEN2*, and *APP*, as well as Aβ peptides. Whereas these studies support the hypothesis that disruption of Ca^{2+} homeostasis contributes to AD, it is difficult to disentangle the effects of familial AD-linked genes on Aβ production from their effects on Ca^{2+} homeostasis. Here, we developed a system in which cellular Ca^{2+} homeostasis could be directly manipulated to study the effects on amyloid precursor protein metabolism and Aβ production. We overexpressed stromal interaction molecule 1 (STIM1) and Orai1, the components of the store-operated Ca^{2+} entry pathway, to generate cells with constitutive and store depletion-induced Ca^{2+} entry. We found striking effects of Ca^{2+} entry induced by overexpression of the constitutively active $STIM1_{D76A}$ mutant on amyloid precursor protein metabolism. Specifically, constitutive activation of Ca^{2+} entry by expression of $STIM1_{D76A}$ significantly reduced Aβ secretion. Our results suggest that disruptions in Ca^{2+} homeostasis may influence AD pathogenesis directly through the modulation of Aβ production.

Alzheimer disease (AD)[3] is a progressive neurodegenerative disorder, the number one cause of dementia in the elderly and the sixth leading cause of death in the United States (1). Pathologically, AD is characterized by the accumulation of 38–43-amino acid-long amyloid β peptides (Aβ) in senile plaques and the presence of tangles composed of hyperphosphorylated tau in the brains of affected individuals (2). Clinically, >90% of cases of AD are classified as non-familial or sporadic disease, with aging as the main risk factor. However, causative mutations leading to early-onset familial AD have been identified in three genes: *APP*, *PSEN1*, and *PSEN2* (3). These mutations all appear to lead to AD by increasing overall levels of Aβ or by promoting production of Aβ peptides ($A\beta_{42}$) that are more prone to oligomerization and deposition. As such, the "amyloid cascade" hypothesis of AD was developed, and Aβ is still considered to be one of, if not the most, important factors in the pathogenesis of AD (4).

Aβ peptides are generated through sequential proteolytic cleavage of amyloid precursor protein (APP), which is a type I transmembrane protein (5). In the Aβ-producing amyloidogenic pathway, APP is first cleaved by the aspartyl protease β-secretase (β-site APP-cleaving enzyme (BACE1)) within its extracellular domain, liberating the soluble ectodomain sAPPβ and generating a membrane-tethered β-C-terminal fragment (β-CTF) (6). The β-CTF is then cleaved within its transmembrane domain by γ-secretase, releasing Aβ and the cytoplasmic APP intracellular domain (AICD). γ-Secretase is an unusual aspartyl protease made up of four transmembrane subunits: nicastrin, APH-1, PEN-2, and presenilin (PS) 1 or PS2 (7). The β-CTF is cleaved serially by γ-secretase at multiple sites producing Aβ fragments of varying size, with $A\beta_{40}$ and $A\beta_{42}$ being

* This work was supported, in whole or in part, by National Institutes of Health Grants AG021495 and AG019070 (to G. T.) and National Research Service Award NS065660 (to W. Z.). This work was also supported by grants from the Alzheimer's Association (to G. T. and K. S. V.).
[S] This article contains a supplemental movie.
[1] To whom correspondence may be addressed: Dept. of Pharmacological and Physiological Sciences, The University of Chicago, Abbott 102, 947 E. 58th St., Chicago, IL 60637. Tel.: 773-702-9334; Fax: 773-834-4522; E-mail: mvillere@bsd.uchicago.edu.
[2] To whom correspondence may be addressed: Dept. of Neurobiology, The University of Chicago, Knapp Bldg. R212, 924 East 57th St., Chicago, IL 60637. Tel.: 773-834-3752; Fax: 773-834-3808; E-mail: gopal@uchicago.edu.

[3] The abbreviations used are: AD, Alzheimer disease; Aβ, amyloid β peptide; APP, amyloid precursor protein; AICD, APP intracellular domain; BACE1, β-site APP-cleaving enzyme; CTF, C-terminal fragment; PS, presenilin; SOCE, store-operated Ca^{2+} entry; STIM1, stromal interaction molecule 1; Tg, thapsigargin; TIRF, total internal reflection microscopy; Tricine, *N*-[2-hydroxy-1,1-bis(hydroxymethyl)ethyl]glycine; 2-APB, 2-aminoethyldiphenyl borate; ER, endoplasmic reticulum; HBSS, Hanks' balanced salt solution.

the most abundant (5). Alternatively, APP can be processed in a non-amyloidogenic manner. Cleavage by α-secretase generates sAPPα and an α-CTF, which is further cleaved by γ-secretase to produce the small peptide p3 and AICD (5). Because α-secretase processing precludes formation of Aβ, the non-amyloidogenic processing of APP is thought to be potentially beneficial.

Multiple lines of evidence suggest that Ca^{2+} homeostasis is deregulated in AD (8, 9). For example, alterations in the levels of Ca^{2+} channels, exchangers, and Ca^{2+}-dependent enzymes have been demonstrated in the brains of affected patients (10–12). Several studies have also found altered Ca^{2+} homeostasis in fibroblasts isolated from patients with AD compared with controls (13–15). In fact, both PS1 and APP have been shown to mediate changes in Ca^{2+} homeostasis. Recent studies have proposed a variety of functions for PS1 in Ca^{2+} homeostasis, including modulation of store-operated Ca^{2+} entry (SOCE), formation of ER Ca^{2+} leak channels, and regulation of sarcoendoplasmic reticulum calcium transport ATPase, inositol trisphosphate receptors, and ryanodine receptors (16–21). APP appears to have numerous effects on Ca^{2+} homeostasis as well. Expression of full length APP, for instance, affects spontaneous Ca^{2+} oscillations in cultured neurons (22, 23). Effects on intracellular Ca^{2+} stores, on the other hand, have been attributed to the APP cleavage product AICD (24, 25). Perhaps most intriguingly of all, however, are the effects mediated directly by the interaction of Aβ with Ca^{2+}-permeable channels. These include functional alterations of plasma membrane ion channels such as voltage-gated Ca^{2+} channels, nicotinic acetylcholine channels, and glutamate, serotonin, and dopamine receptors, alterations of intracellular Ca^{2+} channels such as ryanodine receptors and inositol trisphosphate receptors, and even the direct formation of Ca^{2+}-permeable ion channels (26).

Although a role for disruptions in Ca^{2+} homeostasis in the pathogenesis of AD has been studied in the past using pharmacological manipulations, the effects of these changes on the processing of APP to generate Aβ are not well understood due to conflicting results. Therefore, we devised a genetic approach to alter $[Ca^{2+}]_i$ levels that would allow us to more precisely investigate the effects of Ca^{2+} influx on Aβ generation. Recently, stromal interaction molecule *1* (STIM1) and Orai1 have been identified as the molecular components of the SOCE machinery. STIM1 is a type I transmembrane protein that resides within the ER membrane as dimers under basal conditions. Upon ER Ca^{2+} store depletion, STIM1 rapidly oligomerizes and translocates within the ER membrane to plasma-membrane adjacent regions where it binds, clusters, and activates the store-operated Ca^{2+} channel Orai1 (27, 28). Coexpression of these components is sufficient to reconstitute and potentiate SOCE (29–31). Additionally, expression of a well characterized mutant of the luminal EF-hand domain of STIM1, $STIM1_{D76A}$, leads to constitutive activation of Ca^{2+} influx even under store-replete conditions (32). Therefore, we utilized these components of the SOCE pathway to specifically modulate Ca^{2+} influx and isolate the effects of these manipulations on Aβ generation in the absence of confounding mutations in *PSEN* genes or the use of non-physiologic pharmacologic agents. In particular, we found that increased Ca^{2+} influx resulting from overexpression of the constitutively active $STIM1_{D76A}$ mutant led to dramatic reductions in the secretion of Aβ. Our results indicate that Ca^{2+} influx pathways have multiple effects on APP maturation and processing and provide insights into the importance of Ca^{2+} homeostasis to neuronal pathophysiology and AD.

EXPERIMENTAL PROCEDURES

Cells, Plasmids, and Antibodies—Cells were cultured in DMEM supplemented with 10% bovine growth serum (Hyclone). Human embryonic kidney HEK293 (HEK) cells stably expressing c-Myc epitope-tagged wild-type APP695 (HEK-APP) and APP695 harboring the "Swedish" double mutation (HEK-APPswe) have been previously described (33). The YFP-STIM1 and YFP-$STIM1_{D76A}$ expression vectors were used for transient expression of STIM1 (32). For stable expression of Orai1, the $Orai1_{myc}$ cDNA was subcloned into the pMXs-puro retroviral expression vector (provided by Dr. Toshio Kitamura (University of Tokyo)). Phoenix packaging cells (ATCC) were used to generate retroviruses, and stably transduced pools of HEK-Orai, HEK-APP-Orai, and HEK-APPswe-Orai cells were selected in the presence of 1 μg/ml puromycin. The pMX-C99–6myc plasmid has been previously described (34). Rabbit polyclonal antisera against STIM1, APP, PS1, and Flotillin-2 were previously generated in our laboratory and have been described (35–38). The following antibodies were purchased: anti-Nicastrin (Santa Cruz), mAb 9E10 (ATCC), anti-protein disulfide isomerase (Stressgen), and mAb 4G8 (Covance).

Protein Analysis—For immunoblotting, cells were lysed in cold lysis buffer (50 mM Tris-HCl (pH 7.4), 150 mM NaCl, 0.5% Nonidet P-40, 0.5% sodium deoxycholate, 0.25% sodium dodecyl sulfate, 5 mM EDTA, and protease inhibitor mixture (1:200; Sigma)) and briefly sonicated. Aliquots of lysates were fractionated by SDS-PAGE on 4–20% Tris-glycine gradient gels (Invitrogen) or 16.5% Tris-Tricine gels for APP CTF and Aβ analysis and transferred to polyvinylidene difluoride membranes (Millipore). The membranes were sequentially incubated with primary antibodies and horseradish peroxidase-conjugated protein A (Sigma) or goat anti-mouse IgG (Jackson ImmunoResearch Laboratories), and signals were visualized by enhanced chemiluminescence detection (PerkinElmer Life Sciences). Alternatively, the blots were incubated with IR-dye-conjugated secondary antibodies and visualized by the Odyssey infrared imaging system (LI-COR Biosciences) as described (39).

Analysis of APP processing by metabolic labeling with [^{35}S]Met/Cys was performed as previously described (40). CTM1 antiserum was used to immunoprecipitate full-length APP and APP CTFs from cell lysates, and mAb 4G8 was used to immunoprecipitate Aβ and p3 from conditioned media (40).

Immunofluorescence Microscopy—HEK cells were grown on poly-L-lysine-coated coverslips and transfected with YFP-STIM1 or YFP-$STIM1_{D76A}$. After ~36 h cells were either washed in Hanks' balanced salt solution (HBSS) and fixed in 4% paraformaldehyde or treated with 1 μM thapsigargin in 0 Ca^{2+} HBSS for 10 min before fixation. Cells were permeabilized with 0.2% Triton X-100, and immunofluorescence staining was performed using mAb 9E10 (0.2 μg/ml) and anti-protein disulfide isomerase (1:5000) as described (35). HEK-Orai1 cells were also double-stained with 7 μg/ml wheat germ agglutinin-rhodamine (Vector Laboratories). Alexa Fluor-555 or 647-conju-

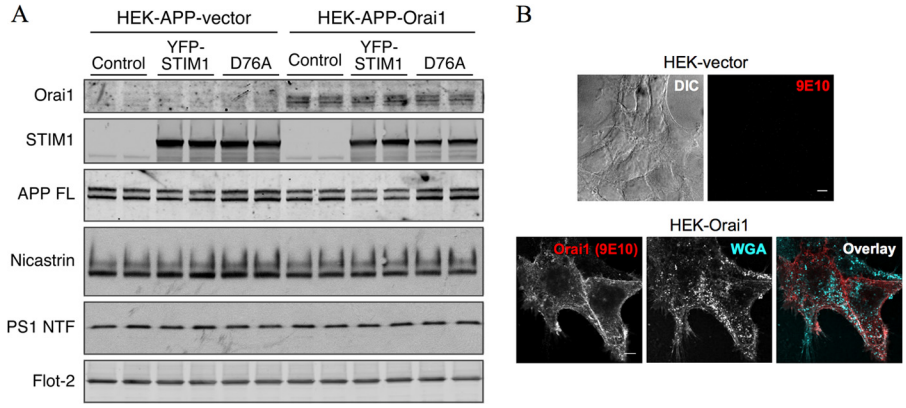

FIGURE 1. **Overexpression of the SOCE machinery in HEK-APP cells.** *A*, HEK-APP cells were stably transduced with recombinant retrovirus containing empty vector or Orai1$_{myc}$ cDNA followed by transient transfection with YFP-STIM1 or YFP-STIM1$_{D76A}$ expression plasmids. Expression of Orai1$_{myc}$, YFP-STIM1, and YFP-STIM1$_{D76A}$ was analyzed by Western blotting. In addition, the levels of full-length APP (*APP FL*), nicastrin, PS1 N-terminal fragment, and flotillin-2 (*Flot-2*) were analyzed. *B*, stable HEK-vector and HEK-Orai1 cells were immunostained with mAb 9E10 to detect Myc-tagged Orai1. Cells were incubated with fluorescent wheat germ agglutinin (*WGA*) before permeabilization to stain surface glycoproteins and glycolipids. *DIC*, differential interference contrast. *Scale bars*, 5 μm.

gated secondary antibodies (Molecular Probes) were used at 1:500 and 1:250 dilutions, respectively. Images were acquired on Leica SP5II STED-CW Superresolution laser confocal microscope using100× objective (NA 1.4; zoom 2.5) and processed using ImageJ software.

For total internal reflection microscopy (TIRF), HEK-APP cells plated on poly-L-lysine-coated 35-mm glass-bottom dishes were transfected with YFP-STIM1 or YFP-STIM1$_{D76A}$. After ~24 h cells were placed in warm HBSS before mounting on the microscope stage maintained at 37 °C using a custom-designed environment chamber. TIRF images were acquired every 15 s using a 100× TIRF objective (1.45 NA) and an EMCCD camera (Photometrics Cascade II). After acquiring base-line TIRF images, cells were briefly washed in Ca^{2+}-free (0 Ca^{2+}) HBSS, and ER Ca^{2+} stores were depleted by the addition of 1 μM thapsigargin (Tg). Images were analyzed using Metamorph imaging software.

Ca^{2+} Imaging—Intracellular Ca^{2+} concentration ($[Ca^{2+}]_i$) was measured in cells loaded with 5 μM Fura-2 AM using a Nikon Diaphot inverted epifluorescence microscope and InCyt IM2™ fluorescence imaging system as previously described (38, 41). A three-part protocol was utilized to measure Ca^{2+} entry under basal conditions (Ca^{2+} stores full) and Ca^{2+} entry after Ca^{2+} store depletion. Specifically, after incubation for ~2–3 min in 0 Ca^{2+} HBSS, cells were perfused in HBSS ($[Ca^{2+}]$ = ~1.3 mM) to measure basal Ca^{2+} entry. Then cells were perfused in 0 Ca^{2+} HBSS for 2 min before the addition of 1 μM thapsigargin to deplete ER Ca^{2+} stores. Finally, cell perfusion was switched back to HBSS to trigger SOCE. Individual responses from ~50 cells per coverslip were monitored and averaged. Each experiment was repeated on 2–4 independent coverslips. In some experiments cells were pretreated with 50 μM 2-aminoethyldiphenyl borate (2-APB) during the Fura-2 AM loading and unloading periods (~2 h), and the cells were perfused in HBSS + 50 μM 2-APB for initial Ca^{2+} measurements (7 min). Then cells were perfused with HBSS for 7 min before switching back to HBSS + 50 μM 2-APB.

Aβ ELISA—Conditioned media from transfected HEK cells were collected after overnight incubation, and sAPPα, Aβ$_{40}$, and Aβ$_{42}$ levels were quantified by ELISA using specific monoclonal antibodies for capture (B113 for Aβ$_{40}$, A387 for Aβ$_{42}$, and 5228 for sAPPα) followed by alkaline phosphatase detection with monoclonal antibody B436 and CSPD Sapphire II Luminescence Substrate (Applied Biosystems) (42).

Statistics—All statistical analyses were calculated using Prism software (GraphPad Software, Inc.). Statistical tests used are indicated in the corresponding figure legends. All data are represented as the mean ± S.E.

RESULTS

Generation of a Genetic Model to Modulate Ca^{2+} Influx—To establish a cell culture model for studying the effects of Ca^{2+} influx on APP processing and Aβ production, we generated cell lines overexpressing the components of the SOCE pathway. Specifically, we transduced HEK cells stably overexpressing human wild-type APP with retroviruses carrying empty vector DNA (HEK-APP vector) or a cDNA encoding the store-operated Ca^{2+} channel Orai1 (HEK-APP-Orai1). For individual experiments, we then transiently transfected these cells with empty vector DNA (Control), the store-operated channel activator YFP-STIM1, or the constitutively active YFP-STIM1$_{D76A}$ mutant. Western blot analysis confirmed expression of Orai1 and YFP-STIM1 or YFP-STIM1$_{D76A}$ in these cells (Fig. 1*A*). Importantly, steady state levels of transgene-derived full-length APP were similar between vector transduced cells and cells overexpressing Orai1 and STIM1 (Fig. 1*A*). Additionally, levels of nicastrin and PS1 N-terminal fragment were similar among all groups of cells, indicating that endogenous γ-secretase subunit expression was unaffected by overexpression of the SOCE machinery (Fig. 1*A*). Similar results were obtained for HEK cells stably expressing APPswe (data not shown). Because expression of full-length APP and endogenous γ-secretase components are unaffected by manipulation of the SOCE machinery, we reasoned that these cells would provide a good model for investigating the effects of Ca^{2+} influx on APP processing.

Having established expression of the components of the SOCE pathway, we utilized immunofluorescence staining to characterize their subcellular localization. In accordance with previously reported studies, Orai1 appeared to localize on the surface with little intracellular accumulation (Fig. 1*B*). On the

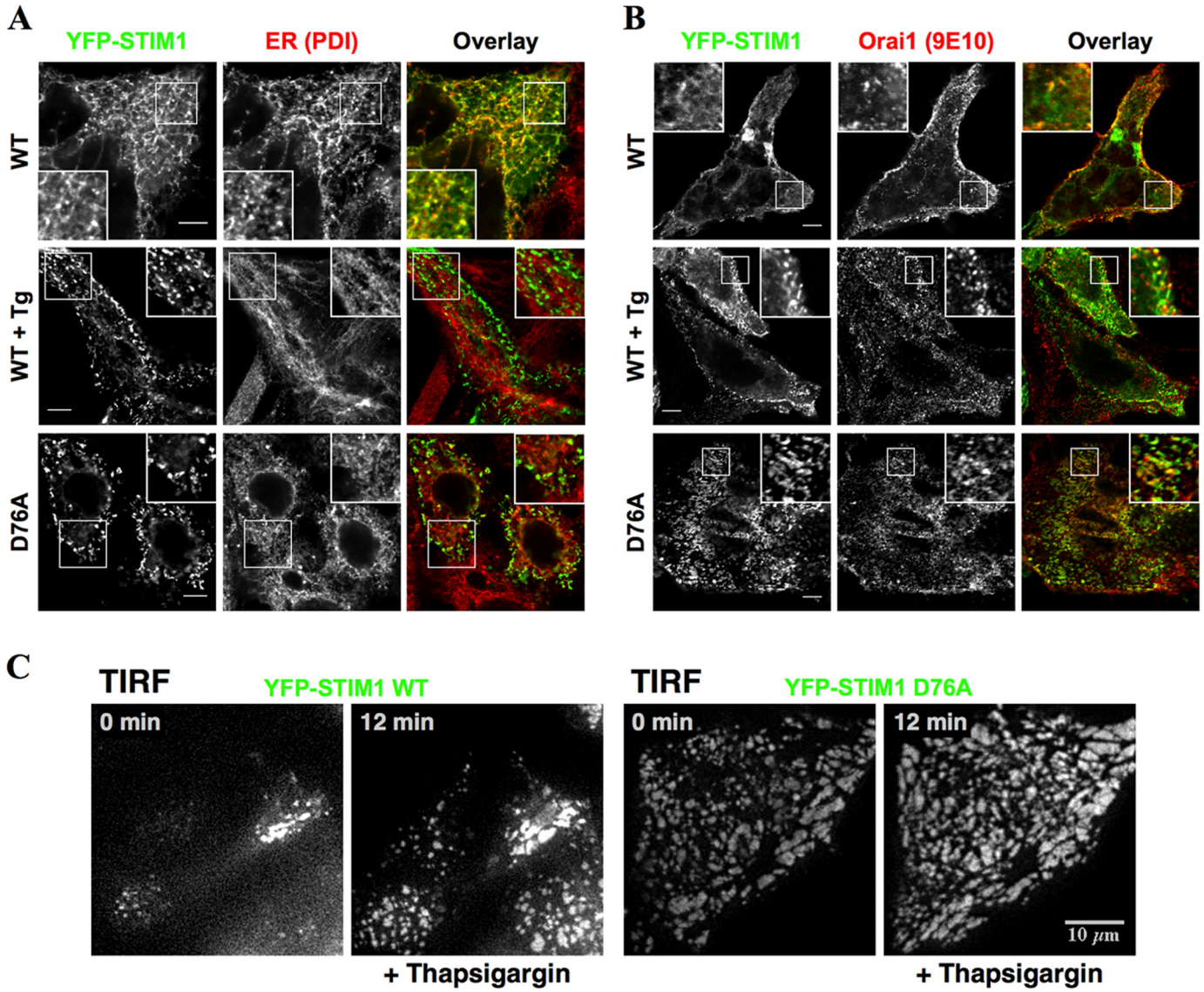

FIGURE 2. **Subcellular localization of YFP-STIM1 and Orai1.** HEK-Orai1 cells transfected with YFP-STIM1 or YFP-STIM1$_{D76A}$ (D76A) were fixed and imaged under basal, ER Ca^{2+} store-replete conditions or after a 10-min treatment with 1 μM Tg in 0 Ca^{2+} HBSS. *A*, cells were immunostained with an antibody against the ER marker, protein disulfide isomerase (*PDI*). *Scale bars*, 5 μm. *B*, cells were immunostained with mAb 9E10 to detect Orai1. *Insets* show enlarged regions indicated by *boxes*. *Scale bars*, 5 μm. *C*, HEK-APP cells transfected with YFP-STIM1 or YFP-STIM1$_{D76A}$ were imaged using TIRF microscopy. Cells were maintained in HBSS in a humidified environment at 37 °C, and images were acquired every 15 s. After 2 min, 1 μM Tg was added in 0 Ca^{2+} HBSS to deplete Ca^{2+} stores. Representative frames from the TIRF image sequence taken before (0 min) and 10 min after the addition of Tg (12 min) are shown.

other hand, YFP-STIM1-transfected cells exhibited a diffuse reticular pattern of fluorescence that overlapped with the ER marker, protein disulfide isomerase (Fig. 2*A*). As expected, YFP-STIM1 fluorescence appeared as multiple discrete puncta after ER Ca^{2+} store depletion with Tg that was distinct from the ER (Fig. 2*A*). In accordance with previous findings (32), STIM1$_{D76A}$ formed puncta even under store-replete conditions (Fig. 2*A*). YFP-STIM1 fluorescence showed some overlap with surface localization of Orai under basal conditions (Fig. 2*B*). After store depletion, obvious overlap between YFP-STIM1 and Orai1 could be observed in discrete puncta. Consistent with previous studies, puncta containing STIM1$_{D76A}$ were also positive for Orai 1 under basal conditions (Fig. 2*B*).

Next, we used TIRF microscopy to observe the dynamic behavior of YFP-STIM1 at sites adjacent to the plasma membrane. Using this approach, we confirmed the dynamic translocation of YFP-STIM1 to plasma-membrane adjacent sites in HEK-APP cells after store depletion with Tg (Fig. 2*C*; supplemental movie, *left panel*). In contrast, after transfection with YFP-STIM1$_{D76A}$, we observed numerous puncta near the plasma membrane under store-replete conditions, and the sizes of these puncta were not significantly affected by store depletion (Fig. 2*C*; supplemental movie, *right panel*). These results confirm that STIM1 and STIM1$_{D76A}$ are not only expressed but also dynamically localize as expected in our cell culture model.

STIM1$_{D76A}$ Alters Ca^{2+} Homeostasis in HEK-APP Cells—Next, we loaded cells with Fura-2 AM and directly measured $[Ca^{2+}]_i$ levels. Because the EF-hand mutation of STIM1, STIM1$_{D76A}$, activates SOCE independently of ER store depletion, we used a three-part protocol to measure both store-dependent (SOCE) and store-independent Ca^{2+} influx (Fig. 3, *A* and *D*). First, cells were switched from perfusion in 0 Ca^{2+}

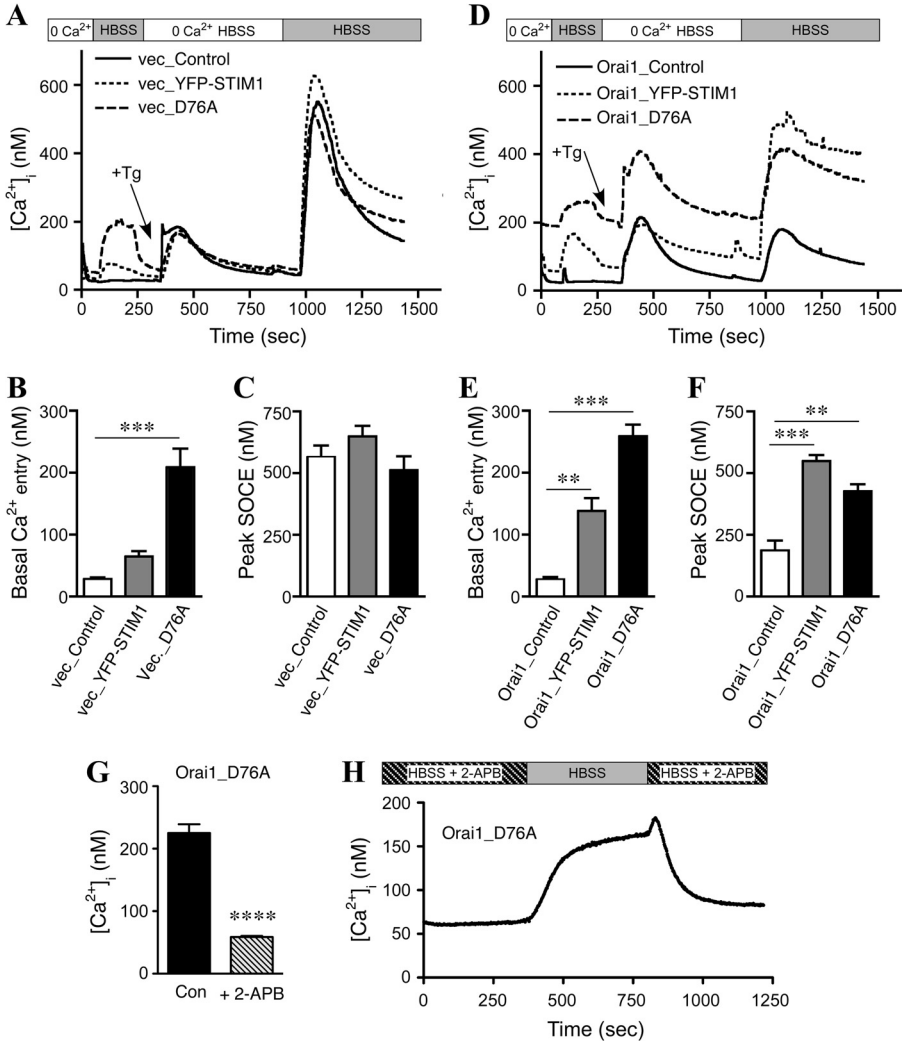

FIGURE 3. **Characterization of calcium entry in HEK-APP and HEK-APP-Orai1 cells.** *A*, Fura-2 AM-loaded HEK-APP cells were imaged to quantify Ca^{2+} entry phenotypes induced by YFP-STIM1 or YFP-$STIM1_{D76A}$ expression. First, cells were switched from 0 Ca^{2+}HBSS to HBSS to assess basal Ca^{2+} levels. Subsequently 1 μM Tg was added in 0 Ca^{2+}HBSS to deplete Ca^{2+} stores followed by calcium add-back to trigger SOCE. *B* and *C*, shown is quantification of the plateau of basal Ca^{2+} entry (*B*) and peak SOCE (*C*) in HEK-APP cells. *D*, Fura-2 AM loaded HEK-APP-Orai cells were imaged as in *A*. *E* and *F*, shown is quantification of basal Ca^{2+} entry (*E*) and peak SOCE (*F*) in HEK-APP-Orai1 cells. Data represent 3–4 experiments, with ~50 cells per experiment; one-way analysis of variance; **, $p < 0.01$; ***, $p < 0.001$. *G*, HEK-APP-Orai1 cells transiently expressing $STIM1_{D76A}$ were pretreated with 50 μM 2-APB for 2 h during the Fura-2 loading and unloading period, the cells were transferred to the imaging chamber containing HBSS + 2-APB, and the basal Ca^{2+} levels recorded. The effect of 2-APB addition on the basal Ca^{2+} levels is plotted; unpaired *t* test with Welch's correction; ****, $p < 0.0001$. *H*, HEK-APP-Orai1 cells transiently expressing STIM1D76A were pretreated with 50 μM 2-APB as above, and the basal Ca^{2+} levels recorded. The cells were then perfused with HBSS for 7 min, and then 2-APB was added back to the chamber. The *trace* represents the mean of six experiments, with ~50 cells per experiment.

HBSS to HBSS to measure store-independent, basal Ca^{2+} entry. After $[Ca^{2+}]_i$ levels plateaued, cells were perfused in 0 Ca^{2+} HBSS, and 1 μM Tg was added to deplete ER Ca^{2+} stores followed by Ca^{2+} add-back in HBSS to trigger SOCE. The plateau for basal Ca^{2+} entry (Fig. 3, *B* and *E*) and the peak for SOCE (Fig. 3, *C* and *F*) were then quantified for each stable cell pool. In vector-transduced HEK-APP cells, overexpression of YFP-STIM1 produced a small, but non-significant potentiation of basal Ca^{2+} entry, whereas overexpression of YFP-$STIM1_{D76A}$ dramatically increased basal Ca^{2+} entry (Fig. 3*B*). Upon Ca^{2+} add-back, robust SOCE was induced in all cases without any discernible difference between the three groups (Fig. 3*C*).

Consistent with previous reports showing a dominant negative effect of expression of Orai1 alone (29, 31), HEK-APP-Orai1 cells, which stably overexpress Orai1, had reduced SOCE (Fig. 3*F*) as compared with parental HEK-APP cells (Fig. 3*C*; Table 1). The transient expression of YFP-STIM1 in HEK-APP-Orai1 cells produced a modest increase in basal Ca^{2+} entry and a large increase in SOCE compared with the transient transfection control (HEK-APP-Orai1 cells transfected with an empty vector), as expected (Fig. 3, *E* and *F*). The transient expression of YFP-$STIM1_{D76A}$ in HEK-APP-Orai1 cells, in contrast, led to dramatic increases in basal Ca^{2+} entry along with significantly elevated basal $[Ca^{2+}]_i$ levels even in 0 Ca^{2+} HBSS (Fig. 3, *D–F*). Similar alterations in Ca^{2+} homeostasis were observed in HEK-APPswe cells (Fig. 4). Thus, our data demonstrate significant modulation of Ca^{2+} homeostasis in these cells (summarized in Table 1), with the most dramatic changes observed in cells expressing $STIM1_{D76A}$.

To confirm that the elevated basal Ca^{2+} levels in the HEK-APP-Orai1 cells transiently expressing YFP-$STIM1_{D76A}$ were indeed the result of elevated SOCE, the effect of the SOCE

TABLE 1
Summary of changes in Ca^{2+} homeostasis in HEK-APP cells

Protein expression	Basal $[Ca^{2+}]_i$	Basal Ca^{2+} entry (plateau)	SOCE peak
	nM	nM	nM
Vector_Control	30.4	28.0	565.5
Vector_YFP-STIM1	42.7	65.2	649.2
Vector_YFP-STIM1$_{D76A}$	54.5	209.3	513.0
Orai_Control	29.4	27.4	187.0
Orai _YFP-STIM1	60.9	138.1	548.6
Orai _YFP-STIM1$_{D76A}$	191.7	259.0	426.9

inhibitor 2-APB was investigated. Cells were pretreated with 50 μM 2-APB during the Fura-2 loading and unloading periods, and the cells were placed in HBSS + 50 μM 2-APB for the initial Ca^{2+} measurements. The high basal levels are clearly inhibited by 2-APB as seen in the statistical comparison of Ca^{2+} basal levels in HEK-APP-Orai1-YFP-STIM1$_{D76A}$ cells in the presence and absence of 2-APB (Fig. 3*G*). Furthermore, the Ca^{2+} levels in these cells dynamically changed when 2-APB was removed for a brief period and then added back (Fig. 3*H*).

It is interesting to note that although the transient expression of STIM1 significantly potentiated SOCE in HEK-APP-Orai1 cells, the overall magnitude of SOCE was not increased compared with HEK-APP cells transiently expressing STIM1 (Fig. 3, *F versus C*; Table 1). Previously published data (29–31) in HEK cells overexpressing both Orai1 and STIM1 show much higher levels of SOCE than seen in HEK-APP cells overexpressing Orai1 and STIM1. Our own experiments overexpressing Orai1 and STIM1 in HEK cells (without overexpression of APP) also showed a much higher level of SOCE (Fig. 4*D*), suggesting that the apparent difference in the magnitude of SOCE potentiation by overexpressing Orai1 and STIM1 may result from the overexpression of APP. In support of this notion, we observed that the magnitude of SOCE in HEK-APPswe cells overexpressing Orai1 and STIM1 was also different from that seen in HEK cells overexpressing Orai1 and STIM1 (Fig. 4).

STIM1$_{D76A}$ Expression Leads to Accumulation of APP CTFs and Reduced Aβ Secretion—Having confirmed significant alterations in Ca^{2+} homeostasis in our cell culture system, we began to investigate the effects of these changes on APP processing. First, we performed Western blot analyses to assess the steady-state levels of full-length APP and APP CTFs derived from α-secretase and BACE1 processing (α- and β-CTFs, respectively) (Fig. 5*A*). We found that overexpression of YFP-STIM1$_{D76A}$ significantly increased β-CTF levels in both HEK-APP vector and HEK-APP-Orai1 cells compared with control transfection (Fig. 5*B*). Similarly, significant accumulation of β-CTFs also occurred in HEK-APPswe-Orai cells after the expression of YFP-STIM1$_{D76A}$ (Fig. 5, *C* and *D*). Although we also observed a trend in the accumulation of α-CTFs after the overexpression of STIM1$_{D76A}$, the difference did not reach statistical significance (Fig. 5). These results raised the possibility that STIM1-mediated alterations in Ca^{2+} homeostasis may have effects on APP processing and/or the fate of APP CTFs.

To further characterize the effects of Orai1 and STIM1 expression on APP processing, we performed metabolic labeling in the HEK-APP vector and HEK-APP-Orai1 cells transfected with YFP-STIM1$_{D76A}$ (Fig. 6, *left panels*). In parallel, we also transfected HEK-APPswe vector and HEK-APPswe-Orai1 cells with YFP-STIM1$_{D76A}$ (Fig. 6, *right panels*). As described above, expression of YFP-STIM1$_{D76A}$ alone or coexpression with Orai1 results in significantly elevated levels of Ca^{2+} entry, even in the absence of store depletion (Figs. 3 and 4, Table 1). We first measured APP synthesis by pulse-labeling cells for 15 min with [^{35}S]Met/Cys and found similar levels of immature full-length APP in control and STIM1$_{D76A}$-transfected cells (Fig. 6). After 3 h of continuous labeling [^{35}S]Met/Cys, we observed similar overall levels of full-length APP among groups but found that compared with control cells, STIM1$_{D76A}$-transfected cells had a shift in the ratio of mature to immature APP, favoring immature APP (Fig. 6). In contrast, steady-state levels of mature and immature APP were similar across cells lines (Figs. 1*A* and 4*A*), suggesting a delay rather than an absolute blockade in APP maturation induced by elevation of $[Ca^{2+}]_i$ levels.

Next, we immunoprecipitated APP CTFs from lysates of cells after 3 h of continuous labeling using the APP C-terminal-specific antibody CTM1. We observed a small but reproducible increase in both α- and β-CTFs in STIM1$_{D76A}$-transfected cells (Fig. 6), consistent with the analysis of steady-state APP CTFs in these cells (Fig. 5). To examine the levels of secreted Aβ-related peptides, we then subjected conditioned media from these experiments to immunoprecipitation using monoclonal antibody 4G8. Notably, in cells transfected with STIM1$_{D76A}$, we observed decreased levels of secreted Aβ (Fig. 6) both from cells stably expressing wild-type APP and from cells expressing APPswe. Furthermore, in STIM1$_{D76A}$-transfected cells expressing APPswe we were also able to observe decreases in secretion of the alternate β-site cleavage-derived product Aβ_{11-40} and a corresponding increase in the levels of α-secretase cleavage-derived p3 peptide (Fig. 6, long exposure (*long exp.*)). Unfortunately, the levels of Aβ_{11-40} and p3 were too low to detect in cells expressing wild-type APP. Importantly, overall protein secretion was not reduced in STIM1$_{D76A}$-transfected cells (data not shown), suggesting that the observed effects on Aβ secretion are not due to a generalized impairment in secretory protein trafficking or secretion of lumenal cargo.

To confirm the results observed in our metabolic labeling experiments, we collected media conditioned by HEK-APP and HEK-APP-Orai1 cells after transfection with YFP-STIM1$_{D76A}$ and quantified levels of Aβ_{40}, Aβ_{42}, and sAPPα by ELISA. In both wild-type APP- and APPswe-expressing cells, elevation of $[Ca^{2+}]_i$ levels by transfection of STIM1$_{D76A}$ produced significant decreases in the amount of secreted Aβ_{40} and Aβ_{42} (Fig. 7, *A* and *C*). Transfection of STIM1$_{D76A}$ also resulted in increased secretion of sAPPα in cells expressing APPswe, although no increase in sAPPα levels was detected in cells expressing wild-type APP (Fig. 7, *B* and *D*).

Based on the observations from metabolic labeling experiments, we reasoned that accumulation of APP CTFs and diminution of Aβ secretion by elevation of $[Ca^{2+}]_i$ levels in cells expressing STIM1$_{D76A}$ might be due to reduced γ-secretase processing of APP β-CTFs. However, it was also possible that elevated $[Ca^{2+}]_i$ levels independently influenced BACE1 and γ-secretase processing. To directly test the effects of $[Ca^{2+}]_i$ levels on γ-secretase processing, we co-transfected HEK cells stably expressing Orai1 with YFP-STIM1$_{D76A}$ and a plasmid

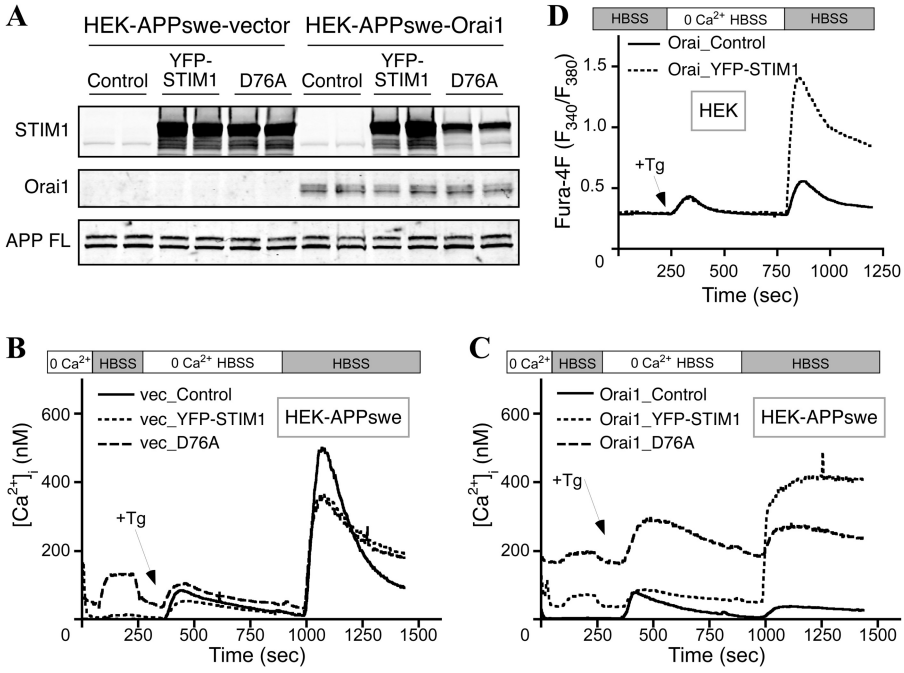

FIGURE 4. **Generation and characterization of Ca^{2+} homeostasis in HEK-APPswe cells.** *A*, HEK cells stably expressing APPswe were transduced with empty vector or $Orai1_{myc}$ followed by transient transfection with YFP-STIM1 or YFP-$STIM1_{D76A}$. Western blot analysis confirmed successful expression of $Orai1_{myc}$, YFP-STIM1, or YFP-$STIM1_{D76A}$, and APPswe. *B* and *C*, Fura-2 AM-loaded HEK-APPswe (*B*) and HEK-APPswe-Orai (*C*) cells were imaged to quantify Ca^{2+} entry phenotypes induced by YFP-STIM1 or YFP-$STIM1_{D76A}$ expression as described in Fig. 2. *D*, stably-transduced HEK-Orai cells (without APP overexpression) were transfected with empty vector control or YFP-STIM1 and subsequently loaded with Fura-4F for Ca^{2+} imaging. After perfusion in HBSS, 1 μM Tg was added in 0 Ca^{2+} HBSS to deplete Ca^{2+} stores followed by perfusion in HBSS to trigger SOCE. Data represent four experiments with ~50 cells per experiment.

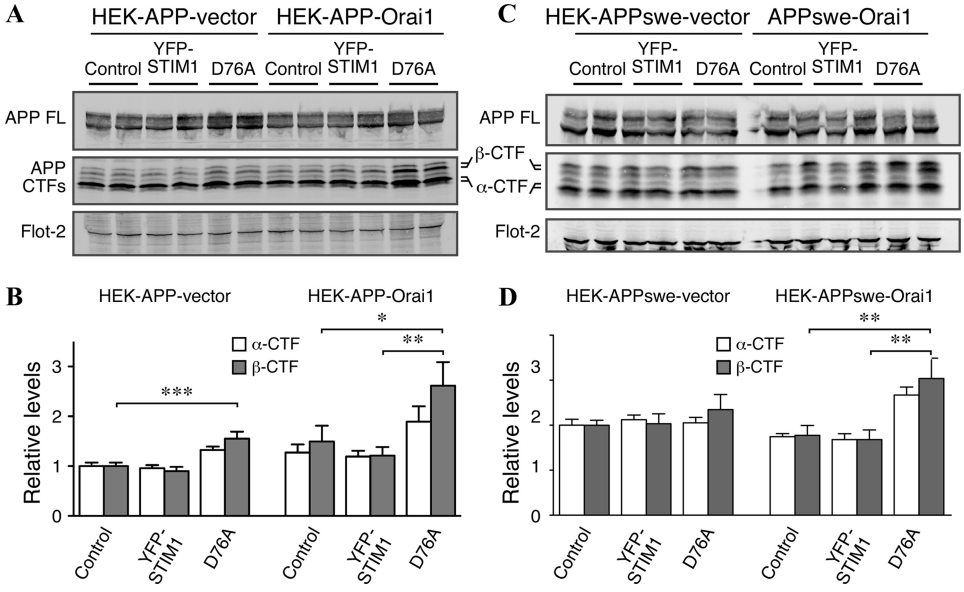

FIGURE 5. **Constitutive activation of SOCE leads to accumulation of APP β-CTFs.** *A*, Western blot analysis of full-length APP and APP CTFs in HEK-APP vector and HEK-APP-Orai1 cells transfected with control, YFP-STIM1, or YFP-$STIM1_{D76A}$ plasmids is shown. *B*, quantification of α- and β-CTF levels, normalized to loading control (Flot-2) HEK-APP-vector cells transfected with control plasmid is shown. *C*, Western blot analysis of transfected HEK-APPswe and HEK-APPswe-Orai1 cells is as described in A. *D*, quantification of α- and β-CTF levels is as described in *B*. Data represent three experiments performed in duplicate; one-way analysis of variance; *, $p < 0.05$; **, $p < 0.01$; ***, $p < 0.001$.

encoding C99–6myc, the APP β-CTF. This construct is often used to examine γ-secretase cleavage of the APP β-CTF in the absence of any confounding effects of α- and β-secretase processing of full-length APP. In agreement with our prediction, we found significantly reduced cleavage of C99 to AICD in cells expressing $STIM1_{D76A}$ compared with controls (Fig. 7*E*). Together, these findings suggest that elevation of $[Ca^{2+}]_i$ levels through the SOCE pathway leads to multiple effects on APP metabolism, including reduced amyloidogenic processing of APP β-CTF by γ-secretase.

DISCUSSION

In recent years several alternative hypotheses to the amyloid cascade have been advanced to explain the synaptic dysfunc-

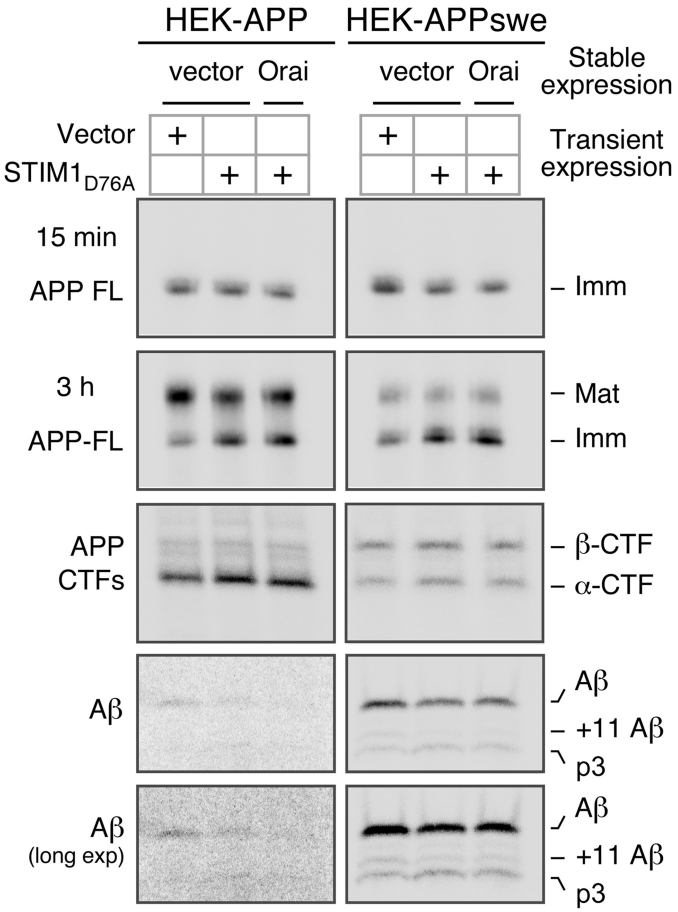

FIGURE 6. **Analysis of APP processing in HEK-APP and HEK-APPswe cells by metabolic labeling.** The indicated HEK cells were transiently transfected with YFP-STIM1$_{D76A}$ and pulse-labeled for 15 min or continuously labeled for 3 h with [^{35}S]Met/Cys. Full-length (*FL*) APP and APP CTFs were immunoprecipitated from cell lysates with CTM1 antibody and analyzed by phosphorimaging. Secreted Aβ was analyzed by immunoprecipitation of conditioned media collected after 3 h labeling and using the monoclonal antibody 4G8. The bands corresponding to Aβ and +11 Aβ, which are generated by BACE1 cleavage at alternate sites followed by γ-secretase cleavage, are indicated. The peptide p3 is released by sequential cleavage of APP by α- and γ-secretases. *Imm*, immature APP; *Mat*, mature APP.

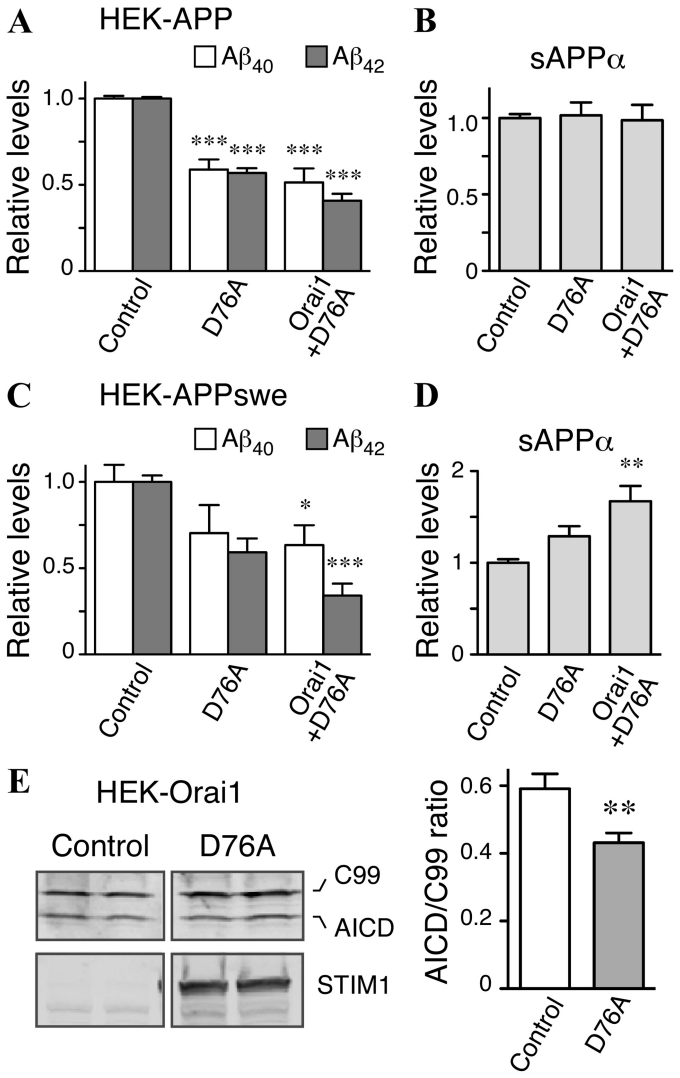

FIGURE 7. **Modulation of SOCE alters levels of secreted Aβ in HEK-APP and HEK-APPswe cells.** *A* and *B*, HEK-APP-vector and HEK-APP-Orai cells were transiently transfected with control plasmid, YFP-STIM1, or YFP-STIM1$_{D76A}$. The levels of Aβ$_{40}$, Aβ$_{42}$ (*A*), and sAPPα (*B*) in conditioned media were quantified by ELISA. *C* and *D*, HEK-APPswe-vector and HEK-APPswe-Orai1 cells were transfected as above, and the levels of secreted Aβ40, Aβ42, and sAPPα were analyzed by ELISA. Data represent three experiments performed in duplicate; one-way analysis of variance; *, $p < 0.05$; **, $p < 0.01$; ***, $p < 0.001$. *E*, HEK cells stably expressing Orai1$_{myc}$ were co-transfected with C99–6myc and either empty vector or YFP-STIM1$_{D76A}$. Western blot analysis of C99 and AICD was then performed using an anti-myc antibody (9E10), and the ratio of AICD:C99 was quantified; $n = 8$ transfections; Student's *t* test; **, $p < 0.01$.

tion and neuronal death that occurs in AD. Dysregulation of Ca^{2+} homeostasis is one such example, and numerous studies have lent support to this hypothesis, from data demonstrating alterations in Ca^{2+} handling in cells from affected patients to the discoveries of molecular roles for presenilins, APP, and Aβ peptides in the regulation of $[Ca^{2+}]_i$ levels (26). Although Ca^{2+} has well established roles in neurotransmission and synaptic plasticity, its effects on the processing of APP and Aβ generation are less well known.

Studies to date have demonstrated conflicting results. In non-excitable cells, pharmacological elevation of $[Ca^{+2}]_i$ has been shown to both increase and decrease Aβ levels (43–45). In neurons, the data on the relationship between Ca^{2+} influx and Aβ production is equally unclear. For example, Tg- and depolarization-induced elevations of $[Ca^{+2}]_i$ have been reported to selectively increase intraneuronal Aβ$_{42}$ (46). Likewise, ionomycin treatment of primary cortical neurons overexpressing human APPswe resulted in an increase in Aβ production through an increase in BACE1 expression (47). In contradiction, familial AD-linked mutations in PS1 that increase Aβ$_{42}$ production were found to decrease SOCE (16). Additionally, Ca^{2+} influx through NMDA receptors has been shown to stimulate non-amyloidogenic α-secretase processing and inhibit Aβ production (48). In general, these studies have been hampered by one of two limitations: modulation of $[Ca^{+2}]_i$ by the expression of PS1 or PS2 mutants, which lends itself to ambiguity as PS1 or PS2 functions as the catalytic subunit of γ-secretase, and the use of non-physiologic pharmacologic agents (Ca^{2+} ionophore, thapsigargin) that often have pleiotropic effects on cellular function.

To avoid these limitations we utilized the molecular components of the SOCE system, STIM1 and Orai1, to genetically alter Ca^{2+} levels in HEK cells. In this way we hypothesized that

we would be able to observe the effects of a primary alteration in Ca^{2+} homeostasis on APP processing in the absence of confounding effects due to presenilin mutations or pharmacologic manipulations. Based on data from previous studies (29–31), we initially expected to observe a potentiation of SOCE in HEK-APP-Orai cells overexpressing STIM1. In contrast to this well characterized effect, we found that the magnitude of SOCE was similar in HEK-APP and HEK-293-APP-Orai1 cells transfected with STIM1. Because we were able to observe STIM1-mediated potentiation of SOCE in HEK-Orai1 cells, but not HEK-APP-Orai1 cells (Figs. 3 and 4), we conclude that this discrepancy is likely attributable to the overexpression of APP. Although numerous papers have demonstrated effects of APP expression on Ca^{2+} homeostasis, the data are often conflicting (24, 25, 49–51). Additionally, no studies to date have examined the effects of APP on SOCE in cells overexpressing STIM1 and Orai1, and thus the exact mechanism by which APP overexpression is affecting this process remains unclear. It will be interesting to further investigate this effect in future studies.

Fortunately, we also utilized the constitutively active $STIM1_{D76A}$ mutant in our study. It is known that expression of this well characterized mutant of the luminal EF-hand domain of STIM1 leads to constitutive activation of Ca^{2+} influx even under store-replete conditions (29, 32). As expected, in co-transfected cells, Orai1 with $STIM1_{D76A}$ oligomerized and formed numerous puncta near the plasma membrane even under store-replete conditions (Fig. 2), in agreement with constitutive Ca^{2+} entry. Indeed, this reconstituted SOCE channel function was inhibited by preincubation with the SOCE blocker, 2-APB (Fig. 3) (31). Although in early studies 2-APB was thought to inhibit inositol trisphosphate receptors in addition to store-operated Ca^{2+} channels, as a result of intense research conducted since the discovery of Orai and STIM family proteins, the complex actions of 2-APB effects on SOCE have been attributed to a direct block of Orai subunits at the channel level as well as an additional uncoupling of STIM1 and Orai subunits (52–57). Thus, the most dramatic derangements in Ca^{2+} homeostasis in HEK-APP-Orai1 cells transfected with $STIM1_{D76A}$ is due to activation of constitutive SOCE. Interestingly, HEK-APP-Orai1 cells transfected with $STIM1_{D76A}$ had significant accumulation of β-CTFs, suggesting potential alterations in APP processing and/or metabolism. Therefore, we chose to focus further investigations of APP processing on these cells with constitutive Ca^{2+} entry. Using metabolic labeling and ELISA we found striking reductions in the secretion of Aβ with concomitant increases in the levels of both α- and β-CTFs. Moreover, we observed reduced APP maturation, a small increase in p3 secretion, and reduced γ-secretase cleavage of APP C99. These results suggest that elevations in $[Ca^{2+}]_i$ levels resulting from constitutive activation of Ca^{2+} entry affects APP metabolism at multiple levels.

Notably, the magnitude of the effect on APP processing we observed appears to be proportional to the level of derangement in cellular Ca^{2+} homeostasis. HEK-APP-Orai1 cells transfected with $STIM1_{D76A}$ exhibited the most prominent elevations in $[Ca^{2+}]_i$ levels to such a degree that resting cytosolic Ca^{2+} levels were significantly elevated even in nominally Ca^{2+}-free buffer. This elevation of basal Ca^{2+} levels suggests significant alterations in the homeostatic mechanisms controlling resting $[Ca^{2+}]_i$ levels. Although this effect has been observed previously, the mechanisms mediating it have not been well characterized (29). However, the alterations in Ca^{2+} homeostatic mechanisms are clearly dependent on the elevated SOCE, as the elevated basal Ca^{2+} levels in HEK-APP-Orai1-YFP-$STIM1_{D76A}$ cells were returned to almost normal levels by preincubating cells for 2 h with 2-APB, a widely used pharmacological agent that (at the concentration used in our study) inhibits SOCE and calcium release-activated Ca^{2+} currents (Fig. 3, *G* and *H*). For the purposes of our study, these dramatic alterations in Ca^{2+} handling were correlated with both greater accumulation of APP CTFs and reduced Aβ generation compared with $STIM1_{D76A}$-transfected cells that do not coexpress Orai1. Therefore, there may be a dose-response relationship between the magnitude of elevation in $[Ca^{2+}]_i$ levels and the impairment in Aβ generation, strengthening the correlation between dysregulation of Ca^{2+} homeostasis and reduced amyloidogenic APP processing.

Throughout our investigations we utilized cells overexpressing wild-type APP and the familial AD-linked Swedish APP mutation. In almost all experiments we found a similar effect of alterations in Ca^{2+} homeostasis on APP metabolism. These include a delay in maturation of APP, accumulation of APP CTFs, reduced secretion of Aβ, and a small increase in p3 levels. The one exception was the effect of $STIM1_{D76A}$ transfection on secretion of sAPPα. In cells expressing APPswe we found that elevation of $[Ca^{2+}]_i$ levels resulted in increased sAPPα secretion, and again greater alterations in Ca^{2+} homeostasis were correlated with larger increases in sAPPα secretion (Fig. 7*D*). However, in cells expressing wild-type APP, $STIM1_{D76A}$ transfection produced no change in secretion of sAPPα (Fig. 7*B*). We suggest that the reason for this difference is likely due to the extent to which full-length APP molecules are subject to amyloidogenic *versus* non-amyloidogenic processing in these cells. Whereas most wild-type APP undergoes non-amyloidogenic processing, the presence of Swedish mutations in APP leads to preferential BACE1 cleavage and consequently a greater proportion of APP undergoing amyloidogenic processing (58). Notably, BACE1 processing of APPswe can occur as early as during transit of nascent APPswe polypeptides through the cis-Golgi (58). Thus, in HEK-APPswe cells even a small reduction in amyloidogenic processing would allow more APP to reach the cell surface and be subject to non-amyloidogenic processing, resulting in a readily observable increase in sAPPα. On the other hand, in HEK-APP-overexpressing cells where most APP is already undergoing non-amyloidogenic processing, further increases in APP available for non-amyloidogenic processing result in a proportionally smaller effect on the total levels of sAPPα produced.

Taken together, our results demonstrate that elevation of $[Ca^{2+}]_i$ levels by Ca^{2+} influx through store-operated channels leads to reduced amyloidogenic processing of APP and a dramatic decrease in the generation of $Aβ_{40}$ and $Aβ_{42}$. Although Aβ has been implicated in the disruption of intracellular Ca^{2+} homeostasis through a variety of mechanisms, including membrane disruption, Ca^{2+} pore formation, and ion channel modulation, our data suggest that the relationship between Ca^{2+}

and Aβ may be reciprocal. Specifically, it appears that Aβ species (peptides, oligomers, and/or fibrils) may lead to elevations in $[Ca^{2+}]_i$ levels that then negatively regulate amyloidogenic APP processing, reducing further production of Aβ. This reciprocity could serve as a protective cellular mechanism, which limits production of Aβ when extracellular concentrations are high, preventing pathologic accumulation of potentially toxic Aβ peptides. Alterations in the mechanisms regulating Ca^{2+} accumulated during aging or through the acquisition of a mutation in *PSEN1* or other AD-associated genes could then potentially disrupt this homeostatic balance, favoring AD pathogenesis. Alternatively, Ca^{2+} induced accumulation of APP CTFs may result in alterations in intracellular signaling, as has been recently demonstrated (59).

In neurons, the principal cell type affected in AD, the relationship between $[Ca^{2+}]_i$ levels and Aβ generation and secretion is likely to be more complex than observed in our experiments in HEK cells. Calcium-regulating systems are markedly more complex in neurons, and Ca^{2+} signals are involved in diverse processes such as protein and secretory vesicle trafficking for neurotransmission, endocytosis, gene transcription, and synaptic plasticity. Neurons are also polarized cells, and many Ca^{2+} signaling events are restricted to specific microdomains. Overall, this results in a system in which the effects of Ca^{2+} signaling on APP processing will depend on the localization, magnitude, and mode of Ca^{2+} entry. For example, in presynaptic nerve terminals Aβ secretion and intraneuronal accumulation of Aβ have been linked to Ca^{2+}-dependent neuronal activity (46, 60). On the other hand, at post-synaptic sites Ca^{2+} influx through NMDA receptors has been reported to reduce Aβ release (48).

We chose to utilize simplified non-neuronal cells for this work precisely because we wanted to avoid the complexity in neuronal Ca^{2+}-regulating systems. Thus, we believe our work presents strong evidence of a direct role for elevated $[Ca^{2+}]_i$ levels in the negative regulation of amyloidogenic APP processing. However, because we utilized the components of the SOCE pathway (STIM1 and Orai1) to manipulate $[Ca^{2+}]_i$ levels, we cannot rule out the possibility that the effects we have observed are specific to STIM1-mediated Ca^{2+} influx through store-operated Ca^{2+} channels. The implications of this possibility on disease pathogenesis are difficult to predict because, although some studies in neurons have demonstrated functional SOCE, the precise roles of STIM1 and Orai1 in the central nervous system remain unknown (61, 62). In fact, STIM1 likely has functions independent of SOCE in neurons as it has been shown to be a negative regulator of voltage-gated Ca^{2+} channels (63, 64). Further studies of the specific role of STIM1 on neuronal Ca^{2+} regulation and APP processing are warranted in the future.

Acknowledgments—We thank Dr. S. Sisodia (University of Chicago) for the HEK-APP and HEK-APPswe cells. The YFP-STIM1 and YFP-STIM1-D76A expression vectors were a generous gift of T. Meyer (Stanford University). The Orai1$_{myc}$ cDNA was a generous gift of M. Prakriya (Northwestern University). Confocal imaging was performed at the Integrated Microscopy Core Facility at the University of Chicago (supported by Grant S10OD010649).

REFERENCES

1. Alzheimer's Association (2012) 2012 Alzheimer's disease facts and figures. *Alzheimers Dement.* **8,** 131–168
2. Selkoe, D. J., Mandelkow, E., and Holtzman, D. M. (2011) *The Biology of Alzheimer Disease*, Cold Spring Harbor Laboratory Press, Cold Spring Harbor, NY
3. Tanzi, R. E., and Bertram, L. (2001) New frontiers in Alzheimer's disease genetics. *Neuron* **32,** 181–184
4. Hardy, J., and Selkoe, D. J. (2002) The amyloid hypothesis of Alzheimer's disease. Progress and problems on the road to therapeutics. *Science* **297,** 353–356
5. Haass, C., Kaether, C., Thinakaran, G., and Sisodia, S. (2012) Trafficking and proteolytic processing of APP. *Cold Spring Harb. Perspect. Med.* **2,** a006270
6. Vassar, R., Kovacs, D. M., Yan, R., and Wong, P. C. (2009) The β-secretase enzyme BACE in health and Alzheimer's disease. Regulation, cell biology, function, and therapeutic potential. *J. Neurosci.* **29,** 12787–12794
7. De Strooper, B., Iwatsubo, T., and Wolfe, M. S. (2012) Presenilins and γ-secretase. Structure, function, and role in Alzheimer Disease. *Cold Spring Harb. Perspect. Med.* **2,** a006304
8. Lindholm, D., Wootz, H., and Korhonen, L. (2006) ER stress and neurodegenerative diseases. *Cell Death Differ* **13,** 385–392
9. Green, K. N., Smith, I. F., and Laferla, F. M. (2007) Role of calcium in the pathogenesis of Alzheimer's disease and transgenic models. *Subcell. Biochem.* **45,** 507–521
10. Colvin, R. A., Bennett, J. W., and Colvin, S. L. (1991) Na^+-Ca^{2+} exchange activity is increased in Alzheimer's disease brain tissues. *Ann. N.Y. Acad. Sci.* **639,** 325–327
11. Grynspan, F., Griffin, W. R., Cataldo, A., Katayama, S., and Nixon, R. A. (1997) Active site-directed antibodies identify calpain II as an early-appearing and pervasive component of neurofibrillary pathology in Alzheimer's disease. *Brain Res* **763,** 145–158
12. Coon, A. L., Wallace, D. R., Mactutus, C. F., and Booze, R. M. (1999) L-type calcium channels in the hippocampus and cerebellum of Alzheimer's disease brain tissue. *Neurobiol. Aging* **20,** 597–603
13. Peterson, C., Ratan, R. R., Shelanski, M. L., and Goldman, J. E. (1988) Altered response of fibroblasts from aged and Alzheimer donors to drugs that elevate cytosolic free calcium. *Neurobiol. Aging* **9,** 261–266
14. Peterson, C., Ratan, R. R., Shelanski, M. L., and Goldman, J. E. (1986) Cytosolic free calcium and cell spreading decrease in fibroblasts from aged and Alzheimer donors. *Proc. Natl. Acad. Sci. U.S.A.* **83,** 7999–8001
15. Hirashima, N., Etcheberrigaray, R., Bergamaschi, S., Racchi, M., Battaini, F., Binetti, G., Govoni, S., and Alkon, D. L. (1996) Calcium responses in human fibroblasts. A diagnostic molecular profile for Alzheimer's disease. *Neurobiol. Aging* **17,** 549–555
16. Yoo, A. S., Cheng, I., Chung, S., Grenfell, T. Z., Lee, H., Pack-Chung, E., Handler, M., Shen, J., Xia, W., Tesco, G., Saunders, A. J., Ding, K., Frosch, M. P., Tanzi, R. E., and Kim, T. W. (2000) Presenilin-mediated modulation of capacitative calcium entry. *Neuron* **27,** 561–572
17. Tu, H., Nelson, O., Bezprozvanny, A., Wang, Z., Lee, S. F., Hao, Y. H., Serneels, L., De Strooper, B., Yu, G., and Bezprozvanny, I. (2006) Presenilins form ER Ca^{2+} leak channels, a function disrupted by familial Alzheimer's disease-linked mutations. *Cell* **126,** 981–993
18. Stutzmann, G. E., Smith, I., Caccamo, A., Oddo, S., Parker, I., and Laferla, F. (2007) Enhanced ryanodine-mediated calcium release in mutant PS1-expressing Alzheimer's mouse models. *Ann. N.Y. Acad. Sci.* **1097,** 265–277
19. Cheung, K. H., Shineman, D., Müller, M., Cárdenas, C., Mei, L., Yang, J., Tomita, T., Iwatsubo, T., Lee, V. M., and Foskett, J. K. (2008) Mechanism of Ca^{2+} disruption in Alzheimer's disease by presenilin regulation of InsP3 receptor channel gating. *Neuron* **58,** 871–883
20. Green, K. N., Demuro, A., Akbari, Y., Hitt, B. D., Smith, I. F., Parker, I., and LaFerla, F. M. (2008) SERCA pump activity is physiologically regulated by presenilin and regulates amyloid β production. *J. Cell Biol.* **181,** 1107–1116
21. Zhang, C., Wu, B., Beglopoulos, V., Wines-Samuelson, M., Zhang, D., Dragatsis, I., Südhof, T. C., and Shen, J. (2009) Presenilins are essential for

regulating neurotransmitter release. *Nature* **460,** 632–636
22. Kloskowska, E., Malkiewicz, K., Winblad, B., Benedikz, E., and Bruton, J. D. (2008) APPswe mutation increases the frequency of spontaneous Ca^{2+}-oscillations in rat hippocampal neurons. *Neurosci. Lett.* **436,** 250–254
23. Santos, S. F., Tasiaux, B., Sindic, C., and Octave, J. N. (2011) Inhibition of neuronal calcium oscillations by cell surface APP phosphorylated on T668. *Neurobiol. Aging* **32,** 2308–2313
24. Hamid, R., Kilger, E., Willem, M., Vassallo, N., Kostka, M., Bornhövd, C., Reichert, A. S., Kretzschmar, H. A., Haass, C., and Herms, J. (2007) Amyloid precursor protein intracellular domain modulates cellular calcium homeostasis and ATP content. *J. Neurochem.* **102,** 1264–1275
25. Leissring, M. A., Murphy, M. P., Mead, T. R., Akbari, Y., Sugarman, M. C., Jannatipour, M., Anliker, B., Müller, U., Saftig, P., De Strooper, B., Wolfe, M. S., Golde, T. E., and LaFerla, F. M. (2002) A physiologic signaling role for the γ-secretase-derived intracellular fragment of APP. *Proc. Natl. Acad. Sci. U.S.A.* **99,** 4697–4702
26. Demuro, A., Parker, I., and Stutzmann, G. E. (2010) Calcium signaling and amyloid toxicity in Alzheimer disease. *J. Biol. Chem.* **285,** 12463–12468
27. Liou, J., Fivaz, M., Inoue, T., and Meyer, T. (2007) Live-cell imaging reveals sequential oligomerization and local plasma membrane targeting of stromal interaction molecule 1 after Ca^{2+} store depletion. *Proc. Natl. Acad. Sci. U.S.A.* **104,** 9301–9306
28. Luik, R. M., Wang, B., Prakriya, M., Wu, M. M., and Lewis, R. S. (2008) Oligomerization of STIM1 couples ER calcium depletion to CRAC channel activation. *Nature* **454,** 538–542
29. Mercer, J. C., Dehaven, W. I., Smyth, J. T., Wedel, B., Boyles, R. R., Bird, G. S., and Putney, J. W., Jr. (2006) Large store-operated calcium selective currents due to co-expression of Orai1 or Orai2 with the intracellular calcium sensor, *Stim1*. *J. Biol. Chem.* **281,** 24979–24990
30. Peinelt, C., Vig, M., Koomoa, D. L., Beck, A., Nadler, M. J., Koblan-Huberson, M., Lis, A., Fleig, A., Penner, R., and Kinet, J. P. (2006) Amplification of CRAC current by STIM1 and CRACM1 (Orai1). *Nat. Cell Biol.* **8,** 771–773
31. Soboloff, J., Spassova, M. A., Tang, X. D., Hewavitharana, T., Xu, W., and Gill, D. L. (2006) Orai1 and STIM reconstitute store-operated calcium channel function. *J. Biol. Chem.* **281,** 20661–20665
32. Liou, J., Kim, M. L., Heo, W. D., Jones, J. T., Myers, J. W., Ferrell, J. E., Jr., and Meyer, T. (2005) STIM is a Ca^{2+} sensor essential for Ca^{2+}-store-depletion-triggered Ca^{2+} influx. *Curr. Biol.* **15,** 1235–1241
33. Kim, S. H., Ikeuchi, T., Yu, C., and Sisodia, S. S. (2003) Regulated hyperaccumulation of presenilin-1 and the "γ-secretase" complex. Evidence for differential intramembranous processing of transmembrane substrates. *J. Biol. Chem.* **278,** 33992–34002
34. Gong, P., Vetrivel, K. S., Nguyen, P. D., Meckler, X., Cheng, H., Kounnas, M. Z., Wagner, S. L., Parent, A. T., and Thinakaran, G. (2010) Mutation analysis of the presenilin 1 N-terminal domain reveals a broad spectrum of γ-secretase activity toward amyloid precursor protein and other substrates. *J. Biol. Chem.* **285,** 38042–38052
35. Vetrivel, K. S., Meckler, X., Chen, Y., Nguyen, P. D., Seidah, N. G., Vassar, R., Wong, P. C., Fukata, M., Kounnas, M. Z., and Thinakaran, G. (2009) Alzheimer disease Aβ production in the absence of *S*-palmitoylation-dependent targeting of BACE1 to lipid rafts. *J. Biol. Chem.* **284,** 3793–3803
36. Thinakaran, G., Regard, J. B., Bouton, C. M., Harris, C. L., Price, D. L., Borchelt, D. R., and Sisodia, S. S. (1998) Stable association of presenilin derivatives and absence of presenilin interactions with APP. *Neurobiol. Dis.* **4,** 438–453
37. Meckler, X., Roseman, J., Das, P., Cheng, H., Pei, S., Keat, M., Kassarjian, B., Golde, T. E., Parent, A. T., and Thinakaran, G. (2010) Reduced Alzheimer's disease β-amyloid deposition in transgenic mice expressing *S*-palmitoylation-deficient APH1aL and nicastrin. *J. Neurosci.* **30,** 16160–16169
38. Zeiger, W., Ito, D., Swetlik, C., Oh-hora, M., Villereal, M. L., and Thinakaran, G. (2011) Stanniocalcin 2 is a negative modulator of store-operated calcium entry. *Mol. Cell. Biol.* **31,** 3710–3722
39. Gong, P., Roseman, J., Fernandez, C. G., Vetrivel, K. S., Bindokas, V. P., Zitzow, L. A., Kar, S., Parent, A. T., and Thinakaran, G. (2011) Transgenic neuronal overexpression reveals that stringently regulated p23 expression is critical for coordinated movement in mice. *Mol. Neurodegener.* **6,** 87
40. Vetrivel, K. S., Barman, A., Chen, Y., Nguyen, P. D., Wagner, S. L., Prabhakar, R., and Thinakaran, G. (2011) Loss of cleavage at β′-site contributes to apparent increase in β-amyloid peptide (Aβ) secretion by β-secretase (BACE1)-glycosylphosphatidylinositol (GPI) processing of amyloid precursor protein. *J. Biol. Chem.* **286,** 26166–26177
41. Wu, X., Zagranichnaya, T. K., Gurda, G. T., Eves, E. M., and Villereal, M. L. (2004) A TRPC1/TRPC3-mediated increase in store-operated calcium entry is required for differentiation of H19-7 hippocampal neuronal cells. *J. Biol. Chem.* **279,** 43392–43402
42. Vetrivel, K. S., Gong, P., Bowen, J. W., Cheng, H., Chen, Y., Carter, M., Nguyen, P. D., Placanica, L., Wieland, F. T., Li, Y. M., Kounnas, M. Z., and Thinakaran, G. (2007) Dual roles of the transmembrane protein p23/TMP21 in the modulation of amyloid precursor protein metabolism. *Mol. Neurodegener.* **2,** 4
43. Buxbaum, J. D., Ruefli, A. A., Parker, C. A., Cypess, A. M., and Greengard, P. (1994) Calcium regulates processing of the Alzheimer amyloid protein precursor in a protein kinase C-independent manner. *Proc. Natl. Acad. Sci. U.S.A.* **91,** 4489–4493
44. Querfurth, H. W., Jiang, J., Geiger, J. D., and Selkoe, D. J. (1997) Caffeine stimulates amyloid β-peptide release from β-amyloid precursor protein-transfected HEK293 cells. *J. Neurochem.* **69,** 1580–1591
45. Querfurth, H. W., and Selkoe, D. J. (1994) Calcium ionophore increases amyloid β peptide production by cultured cells. *Biochemistry* **33,** 4550–4561
46. Pierrot, N., Ghisdal, P., Caumont, A. S., and Octave, J. N. (2004) Intraneuronal amyloid-β1–42 production triggered by sustained increase of cytosolic calcium concentration induces neuronal death. *J. Neurochem.* **88,** 1140–1150
47. Cho, H. J., Jin, S. M., Youn, H. D., Huh, K., and Mook-Jung, I. (2008) Disrupted intracellular calcium regulates BACE1 gene expression via nuclear factor of activated T cells 1 (NFAT 1) signaling. *Aging Cell* **7,** 137–147
48. Hoey, S. E., Williams, R. J., and Perkinton, M. S. (2009) Synaptic NMDA receptor activation stimulates α-secretase amyloid precursor protein processing and inhibits amyloid-β production. *J. Neurosci.* **29,** 4442–4460
49. Chatzistavraki, M., Kyratzi, E., Fotinopoulou, A., Papazafiri, P., and Efthimiopoulos, S. (2013) Down-regulation of AβPP enhances both calcium content of endoplasmic reticulum and acidic stores and the dynamics of store operated calcium channel activity. *J. Alzheimers Dis.* **34,** 407–415
50. Stieren, E., Werchan, W. P., El Ayadi, A., Li, F., and Boehning, D. (2010) FAD mutations in amyloid precursor protein do not directly perturb intracellular calcium homeostasis. *PLoS ONE* **5,** e11992
51. Linde, C. I., Baryshnikov, S. G., Mazzocco-Spezzia, A., and Golovina, V. A. (2011) Dysregulation of Ca^{2+} signaling in astrocytes from mice lacking amyloid precursor protein. *Am. J. Physiol. Cell Physiol.* **300,** C1502–C1512
52. Bootman, M. D., Collins, T. J., Mackenzie, L., Roderick, H. L., Berridge, M. J., and Peppiatt, C. M. (2002) 2-Aminoethoxydiphenyl borate (2-APB) is a reliable blocker of store-operated Ca^{2+} entry but an inconsistent inhibitor of InsP3-induced Ca^{2+} release. *FASEB J.* **16,** 1145–1150
53. Peppiatt, C. M., Collins, T. J., Mackenzie, L., Conway, S. J., Holmes, A. B., Bootman, M. D., Berridge, M. J., Seo, J. T., and Roderick, H. L. (2003) 2-Aminoethoxydiphenyl borate (2-APB) antagonises inositol 1,4,5-trisphosphate-induced calcium release, inhibits calcium pumps, and has a use-dependent and slowly reversible action on store-operated calcium entry channels. *Cell Calcium* **34,** 97–108
54. DeHaven, W. I., Smyth, J. T., Boyles, R. R., Bird, G. S., and Putney, J. W., Jr. (2008) Complex actions of 2-aminoethyldiphenyl borate on store-operated calcium entry. *J. Biol. Chem.* **283,** 19265–19273
55. Peinelt, C., Lis, A., Beck, A., Fleig, A., and Penner, R. (2008) 2-Aminoethoxydiphenyl borate directly facilitates and indirectly inhibits STIM1-dependent gating of CRAC channels. *J. Physiol.* **586,** 3061–3073
56. Schindl, R., Bergsmann, J., Frischauf, I., Derler, I., Fahrner, M., Muik, M., Fritsch, R., Groschner, K., and Romanin, C. (2008) 2-Aminoethoxydiphenyl borate alters selectivity of Orai3 channels by increasing their pore size. *J. Biol. Chem.* **283,** 20261–20267
57. Zhang, S. L., Kozak, J. A., Jiang, W., Yeromin, A. V., Chen, J., Yu, Y., Penna, A., Shen, W., Chi, V., and Cahalan, M. D. (2008) Store-dependent and -independent modes regulating Ca^{2+} release-activated Ca^{2+} channel ac-

tivity of human Orai1 and Orai3. *J. Biol. Chem.* **283,** 17662–17671
58. Thinakaran, G., Teplow, D. B., Siman, R., Greenberg, B., and Sisodia, S. S. (1996) Metabolism of the "Swedish" amyloid precursor protein variant in neuro2a (N2a) cells. Evidence that cleavage at the "β-secretase" site occurs in the Golgi apparatus. *J. Biol. Chem.* **271,** 9390–9397
59. Deyts, C., Vetrivel, K. S., Das, S., Shepherd, Y. M., Dupré, D. J., Thinakaran, G., and Parent, A. T. (2012) Novel $G\alpha_s$-protein signaling associated with membrane-tethered amyloid precursor protein intracellular domain. *J. Neurosci.* **32,** 1714–1729
60. Kamenetz, F., Tomita, T., Hsieh, H., Seabrook, G., Borchelt, D., Iwatsubo, T., Sisodia, S., and Malinow, R. (2003) APP processing and synaptic function. *Neuron* **37,** 925–937
61. Baba, A., Yasui, T., Fujisawa, S., Yamada, R. X., Yamada, M. K., Nishiyama, N., Matsuki, N., and Ikegaya, Y. (2003) Activity-evoked capacitative Ca^{2+} entry. Implications in synaptic plasticity. *J. Neurosci.* **23,** 7737–7741
62. Bouron, A., Altafaj, X., Boisseau, S., and De Waard, M. (2005) A store-operated Ca^{2+} influx activated in response to the depletion of thapsigargin-sensitive Ca^{2+} stores is developmentally regulated in embryonic cortical neurons from mice. *Brain Res. Dev. Brain Res.* **159,** 64–71
63. Park, C. Y., Shcheglovitov, A., and Dolmetsch, R. (2010) The CRAC channel activator STIM1 binds and inhibits L-type voltage-gated calcium channels. *Science* **330,** 101–105
64. Wang, Y., Deng, X., Mancarella, S., Hendron, E., Eguchi, S., Soboloff, J., Tang, X. D., and Gill, D. L. (2010) The calcium store sensor, *STIM1*, reciprocally controls Orai and CaV1.2 channels. *Science* **330,** 105–109